Eur. Phys. J. A **23**, 473–480 (2005)
DOI 10.1140/epja/i2004-10109-6

THE EUROPEAN PHYSICAL JOURNAL A

Fusion-evaporation cross-sections for ^{48}Ca + ^{154}Sm near the Coulomb barrier

Evidence for fusion enhancement and hindrance

A.M. Stefanini[1,a], M. Trotta[2], B.R. Behera[1], L. Corradi[1], E. Fioretto[1], A. Gadea[1], A. Latina[1], S. Szilner[1], Y.W. Wu[1], S. Beghini[3], G. Montagnoli[3], F. Scarlassara[3], A.Yu. Chizhov[4], I.M. Itkis[4], N.A. Kondratiev[4], I.V. Pokrovskiy[4], R.N. Sagaidak[4], G.N. Kniajeva[4], E.M. Kozulin[4], V.M. Voskressensky[4], S. Courtin[5], F. Haas[5], and N. Rowley[5]

[1] INFN - Laboratori Nazionali di Legnaro, viale dell'Università 2, I-35020 Legnaro (Padova), Italy
[2] INFN - Sezione di Napoli and Dipartimento di Fisica, Università di Napoli, Italy
[3] Dipartimento di Fisica, Università di Padova and INFN, Sezione di Padova, Padova, Italy
[4] Flerov Laboratory of Nuclear Reactions, JINR, 141980 Dubna, Moscow region, Russia
[5] IReS, UMR 7500, IN2P3-CNRS/Université Louis Pasteur, B.P. 28, F-67037 Strasbourg Cedex 2, France

Received: 15 October 2004 / Revised version: 20 November 2004 /
Published online: 12 January 2005 –
Communicated by C. Signorini

Abstract. Measurements of fusion-evaporation cross-sections for the system ^{48}Ca + ^{154}Sm have been performed in the sub- and near-barrier energy range. Barrier-passing cross-sections have been obtained by adding recently measured capture-fission cross-sections at the same energies, and the barrier distribution for capture has been extracted. The data have been analyzed within a coupled-channel model, and a large subbarrier cross-section enhancement is observed, due to the ground-state prolate deformation of ^{154}Sm. The ^{48}Ca + ^{154}Sm capture cross-sections are compared to existing data on ^{16}O + ^{186}W fusion, leading to the same CN, where a few higher-energy points have also been measured. The evaporation residue cross-sections for the two systems above the barrier indicate that complete fusion is inhibited for ^{48}Ca + ^{154}Sm by $\approx 40\%$ in that energy region, with respect to ^{16}O + ^{186}W.

PACS. 25.70.-z Low and intermediate energy heavy-ion reactions – 25.70.Jj Fusion and fusion-fission reactions

1 Introduction

The experimental knowledge on fusion between light and medium-heavy nuclei at sub- and near-barrier energies has grown considerably in the last twenty years [1,2]. The theoretical models are able to reproduce and predict the main features of such processes, but properly understanding the fusion dynamics for heavy systems requires many more ingredients. The need for more experimental data to disentangle various concurrent effects, is clearly felt. A full understanding of all steps of the reaction dynamics is very important for the challenging issue of superheavy elements production.

For light or medium-heavy systems, capture inside the Coulomb barrier leads invariably to fusion, so that the capture (or barrier-passing) cross-section coincides with the total fusion cross-section. Total fusion implies the formation of the compound nucleus. However, for heavy systems capture inside the barrier, *i.e.* formation of a di-nucleus, is not a sufficient condition for fusion. The di-nucleus may reseparate into two fragments before that full equilibration of all degrees of freedom has been reached. Consequently, a considerable part of the total capture cross-section is "lost" into the quasi-fission channel. This phenomenon is experimentally observed as a hindrance to fusion [3,4].

Very schematically, fusion enhancements and fusion hindrance phenomena are both present in the interesting energy range near the Coulomb barrier for heavy and very heavy systems. They influence fusion cross-sections in opposite ways, but the underlying phenomena are acting at different stages of the dynamical evolution of the projectile + target system. Channel coupling effects, expected to be very strong in heavy systems, facilitate capture inside the Coulomb barrier. At a slightly later stage, when capture has taken place and the di-nucleus has been formed, its ability to form a real compound nucleus (CN) depends on other (less studied) entrance-channel properties, like energy, mass-asymmetry, nuclear deformation and shell effects.

[a] e-mail: alberto.stefanini@lnl.infn.it

The dependence of fusion hindrance on mass asymmetry in the entrance channel was indicated by early experiments (see, *e.g.*, [5]) and analyzed within the extra-push model [6–8]. In the measurements of Back *et al.* [9], evidence for quasi-fission was found for ^{32}S + ^{182}W, and it was shown that complete fusion is only a small fraction of the total reaction cross-section for ^{48}Ti + ^{166}Er and ^{60}Ni + ^{154}Sm. All three systems lead to the ^{214}Th* CN. More recent measurements on the production of ^{216}Ra* and ^{220}Th* CN [10,11] have shown, in a model-independent way, that fusion is increasingly inhibited near the barrier, for Z_1Z_2 values as low as ≈ 700, when entrance channels have decreasing mass asymmetry, due to the competition with quasi-fission. Those experiments demonstrated that the inhibition exists already for the low partial waves associated with a significant evaporation residue (ER) production.

The influence of nuclear static deformation on the fusion process has been the object of various investigations (see, *e.g.*, [12]). In particular, the fusion barrier distribution of ^{16}O + ^{154}Sm [13] has a characteristic shape due to the prolate deformation of ^{154}Sm. Using this nucleus as the target and a spherical projectile, heavier than ^{16}O, should reveal stronger subbarrier fusion enhancements and a wider barrier distribution. However, one has also evidence that deformation may facilitate the onset of quasi-fission, thereby inhibiting fusion. In ^{60}Ni + ^{154}Sm [14], a strong hindrance to fusion was deduced from the measured subbarrier ER cross-sections. The fusion hindrance was attributed to "tip" collisions with the deformed samarium target at subbarrier energies, following previous evidence for ^{16}O + ^{238}U [15]; no hindrance was observed above the barrier where "side" collisions become energetically possible.

Closed-shell nuclei are usually rigid against quadrupole vibrations. Therefore, couplings with such inelastic states have a small effect on subbarrier fusion probabilities. But couplings to octupole deformations may be strong even in magic nuclei (*e.g.* in ^{40}Ca or in ^{208}Pb), so leading to large cross-section enhancements [16–18]. The case of ^{48}Ca is interesting, since it is very stiff both for quadrupole and for octupole vibrations. Fusion hindrance itself may be affected as well by shell effects in the entrance channel [19,20].

This paper presents the results of our experimental study of fusion of the relatively heavy, magic nucleus ^{48}Ca with the well-deformed target ^{154}Sm. We provide experimental information on fusion dynamics of ^{48}Ca + ^{154}Sm in a large energy range going from well below to well above the Coulomb barrier. Fusion hindrance has been recently observed [21] in the similar, but heavier system ^{48}Ca + ^{168}Er. The purpose of the present work was twofold: 1) to obtain experimental confirmation to the expected large channel coupling effects in the subbarrier energy regime, and to analyze the results within the coupled-channel model; 2) to look for fusion hindrance in a system where Z_1Z_2 is as large as 1240, but the CN ^{202}Pb* is relatively lighter than in previous studies [9–11,14,15,21], and where deformation is present, so to extend our knowledge on the entrance channel properties which may be relevant for the onset of fusion hindrance/quasi-fission.

We have measured the cross-sections for ER production (a clear signature for fusion) for this system. By adding recently measured capture-fission cross-sections in the same energy range, we have deduced total capture (barrier-passing) cross-sections. The barrier distribution has been extracted as the second derivative of the capture excitation function [1]. Both capture cross-sections and barrier distribution have been compared with the predictions of coupled-channel calculations where the static deformation of ^{154}Sm has been taken into account. A relative comparison has also been done with the subbarrier fusion cross-sections of ^{16}O + ^{186}W [12,22]. Above the Coulomb barrier the ^{48}Ca + ^{154}Sm ER cross-sections have been analyzed together with the corresponding data for ^{16}O + ^{186}W, leading to the same CN, where we have also measured a few higher-energy points. The reduced ER cross-sections for the two systems have been compared, looking for a possible fusion hindrance in ^{48}Ca + ^{154}Sm. Part of the present results was presented at recent Conferences [23].

The following section 2 describes the experimental set-up and presents the results. Section 3 is dedicated to the analysis of the capture cross-sections for ^{48}Ca + ^{154}Sm within the coupled-channel model, and to a comparison of capture cross-sections for ^{48}Ca + ^{154}Sm with respect to fusion cross-sections of ^{16}O + ^{186}W. Section 4 shows the ER cross-sections for ^{48}Ca + ^{154}Sm and ^{16}O + ^{186}W in a reduced scale where fusion hindrance effects can be readily put into evidence, in a model-independent way. A summary and the conclusions of the paper are presented in sect. 5.

2 The experiments

2.1 Set-up and procedures

Heavy-ion beams from the XTU Tandem-ALPI accelerator complex of the Laboratori Nazionali di Legnaro of INFN have been used for the experiments reported here. The ^{48}Ca beams were produced by the sputter ion source where a metallic calcium sample, enriched to 50% in mass 48, was sprayed with ammonia and the resulting CaH^- ions were injected into the accelerator. Beam intensities on targets were $\simeq$ 2–5 pnA, depending on the experimental conditions. The energy range for measurements was 163–220 MeV (roughly from 11% below to 20% above the nominal Coulomb barrier). The ^{16}O beams had energies in the range 105–121 MeV with intensities around 10 pnA.

The targets, placed in the center of a $\varnothing$ = 100 cm scattering chamber, were evaporations of metallic ^{154}Sm (50–200 μg/cm^2) and of $^{186}WO_3$ (50 μg/cm^2) on carbon backings (15–20 μg/cm^2) facing the beam, with isotopic enrichments 98.7% and 97.5%, respectively. The beam energy losses in the carbon backings were $\simeq$ 400 keV and $\simeq$ 70 keV for ^{48}Ca and for ^{16}O, respectively, and they were taken into account in the data analysis.

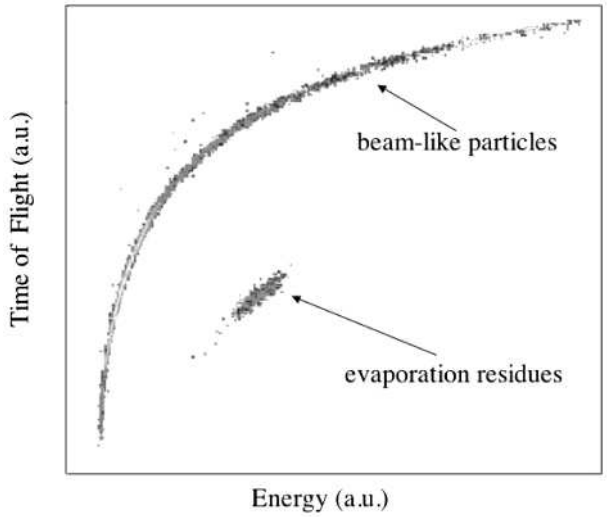

Fig. 1. Energy - Time-of-flight matrix obtained for the reaction ^{48}Ca + ^{154}Sm, at $E_{\rm lab} = 208\,$MeV and $\theta_{\rm lab} = 0°$.

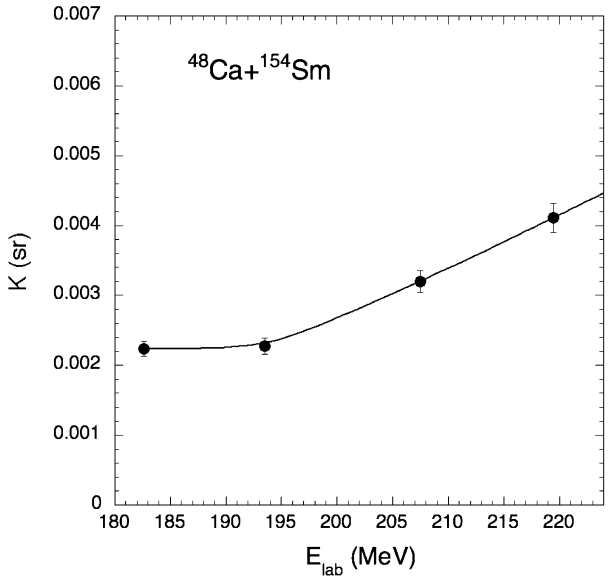

Fig. 2. The ratio K between the total ER cross-section and the differential ER cross-section measured at 0° for ^{48}Ca + ^{154}Sm (see text). The Bass barrier [26] is around 183 MeV. The full line is an interpolation between the measured points.

The nominal beam energy was defined by the 90° analyzing magnet of the XTU Tandem with an uncertainty $\leq 1/800$ [24]. A fluorescent quartz was used to focus the beams to the same position on the targets.

Four silicon detectors monitored continuously the beam intensity and position. They detected Rutherford yields from the target and were placed above and below, and to the left and right of the beam at the same scattering angle $\theta_{\rm lab} = 13°$ or 16°, depending on the run. Small corrections to ER cross-sections were made according to observed variations of the relative yields in the monitors, due to possible changes of beam focusing and position during the various runs.

The forward-recoiling ER were separated from the much stronger flux of beam and beam-like particles by means of an electrostatic deflector [25], installed outside the scattering chamber, with an entrance collimator and two separated pairs of metallic plates $10 \times 25\,$cm^2. The electrostatic field between the plates (perpendicular to the ion direction), deflected beam particles less than ER. While the beam was stopped after the plates, the ER entered a second collimator and were detected by an energy time-of-flight telescope consisting of a micro-channel plate detector (collimated to a 15 mm diameter) and, 40 cm downstream, of a 300 mm^2 silicon surface-barrier detector. Figure 1 shows a two-dimensional time-of-flight *vs.* energy spectrum measured for ^{48}Ca + ^{154}Sm at $\theta_{\rm lab} = 0°$ and $E_{\rm lab} = 208\,$MeV. The group of ER is cleanly separated from the energy-degraded beam-like particles. At the same time, due to the mass resolution of the set-up ($\Delta A/A \simeq 1/50$) we cannot distinguish the individual xn, pxn and αxn evaporation channels from the ^{202}Pb* CN decay.

Besides 0° excitation functions, ER angular distributions were measured for ^{48}Ca + ^{154}Sm at $E_{\rm lab} = 183, 194, 208, 220\,$MeV in the range $-4°$ to $+4°$, and for ^{16}O + ^{186}W at $E_{\rm lab} = 121\,$MeV in the range $-6°$ to $+4°$, with one degree steps.

2.2 Results

Detailed studies of ER excitation functions for ^{16}O + ^{186}W were performed in the past at sub- and near-barrier energies [12,22]. The results of the two experiments are in good agreement with each other. We repeated the measurement of Oak Ridge at $E_{\rm lab} = 105\,$MeV, and extended the experiment to the higher energies $E_{\rm lab} = 109.7, 115.6, 121.1$. The very low energies of the ER in this system make it difficult to estimate the overall efficiency of our set-up (beam deflector and detectors). Consequently, we have normalized the absolute cross-section scale to the point at $E_{\rm lab} = 105\,$MeV ($E^*_{\rm CN} = 75.5\,$MeV), measured in ref. [22]. Starting from that point upwards, the energy dependence of the ER angular distribution width was calculated taking into account, besides the increasing number of evaporated particles, the ER angular straggling in the target and in the carbon foil of the MCP detector. Actually for those ER with very low energy, the dominant factor in determining the angular distribution width is the angular straggling, due to multiple scattering on the atoms of the materials. The calculation gives good agreement with the angular distribution we measured at $E_{\rm lab} = 121\,$MeV.

For ^{48}Ca + ^{154}Sm the set-up efficiency (mainly dependent on the electrostatic filter transmission T in this case) was measured using the same procedure as in previous experiments (see ref. [24] for details) at $E_{\rm lab} = 194, 208$ and 220 MeV. Since no appreciable energy dependence of the transmission was observed within the experimental accuracy, the weighted average value $T = 0.61 \pm 0.05$ was adopted for all ^{48}Ca energies.

The ER cross-sections for ^{48}Ca + ^{154}Sm were obtained by fitting the five measured angular distributions by Gaussian functions (see, *e.g.*, [12]). The ratio K between the

Table 1. Evaporation residue cross-sections for ^{48}Ca + ^{154}Sm measured in the present work. The quoted errors are statistical uncertainties (see text).

$E_{\rm c.m.}$ (MeV)	$\sigma_{\rm ER}$ (mb)	$E_{\rm c.m.}$ (MeV)	$\sigma_{\rm ER}$ (mb)
125.18	0.048 ± 0.029	140.43	36.2 ± 0.7
125.79	0.145 ± 0.039	141.04	41.5 ± 0.8
126.40	0.184 ± 0.039	141.65	50.3 ± 1.0
127.01	0.407 ± 0.058	142.26	55.0 ± 1.0
127.62	0.688 ± 0.087	142.87	60.1 ± 1.0
128.23	1.07 ± 0.096	143.48	62.9 ± 1.1
128.84	1.70 ± 0.12	144.09	66.6 ± 1.2
129.45	1.86 ± 0.12	144.70	69.4 ± 1.2
130.06	2.86 ± 0.15	145.31	76.9 ± 1.6
130.67	3.60 ± 0.16	145.92	81.6 ± 1.7
131.28	4.61 ± 0.19	146.53	88.7 ± 1.8
131.89	5.96 ± 0.25	147.14	88.8 ± 1.5
132.50	7.20 ± 0.30	147.75	88.2 ± 1.6
133.11	8.10 ± 0.32	148.36	95.8 ± 1.8
133.72	9.34 ± 0.29	148.97	97.1 ± 1.8
134.33	11.18 ± 0.39	150.80	103.7 ± 2.1
134.94	11.93 ± 0.36	152.70	111.2 ± 2.2
135.55	14.0 ± 0.4	154.53	107.9 ± 2.4
136.16	15.9 ± 0.5	156.36	115.6 ± 2.5
136.77	17.1 ± 0.5	158.19	110.3 ± 2.4
137.38	19.9 ± 0.6	159.87	107.0 ± 6.1
137.99	22.8 ± 0.7	161.24	105.1 ± 5.3
138.60	26.5 ± 0.8	164.29	102.6 ± 5.3
139.21	31.6 ± 0.6	165.20	99.7 ± 4.6
139.82	34.9 ± 0.6	167.34	102.2 ± 5.8

total area under the Gaussian and the ER differential cross-section at 0° gives the total ER cross-section. This ratio is shown in fig. 2. Interpolated values were used for the energies where no angular distribution was measured. The width of the angular distributions increases significantly above $E_{\rm lab} = 194$ MeV. This is mainly due to the increasing number of neutrons, protons and α-particles evaporated at high CN excitation energies $E^*_{\rm CN}$. The absolute cross-section normalization relies, additionally, on the knowledge of the relevant geometrical solid angles of the detectors ($\simeq 0.025$ msr for the energy time-of-flight telescope) [24]. The ER cross-sections we have obtained for ^{48}Ca + ^{154}Sm are listed in table 1.

3 Capture cross-sections

The capture, or barrier-passing, cross-section we are going to discuss in the following, is the sum of the capture-fission and ER cross-sections. The present ER cross-sections for ^{48}Ca + ^{154}Sm have been summed with the capture-fission cross-sections recently measured in a parallel experiment at LNL [23]. Those fission cross-sections actually include possible quasi-fission contributions besides CN fission, so that the resulting numbers are the total cross-sections for capture inside the Coulomb barrier. They are shown in fig. 3, together with the ER excitation function measured in the present work. The quoted errors are statistical uncertainties only, and they are smaller than the symbol size except for the lowest energies. The absolute ER cross-section scale has a systematic uncertainty of about ±15% [24], mainly due to the uncertainties in the set-up efficiency and ER angular distributions measurements. The overall error in the fission cross-sections [23] is near to ±10%.

Since fission cross-sections are negligible at very low energies, capture and ER cross-sections are practically

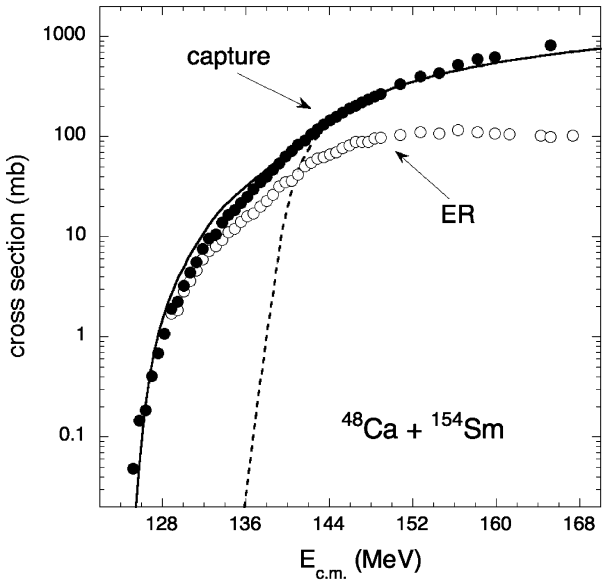

Fig. 3. Capture (full dots) and ER (open dots) excitation functions for ^{48}Ca + ^{154}Sm. The full line is the result of the CC calculations discussed in the text. The dotted line shows the no-coupling limit (one-dimensional barrier tunnelling).

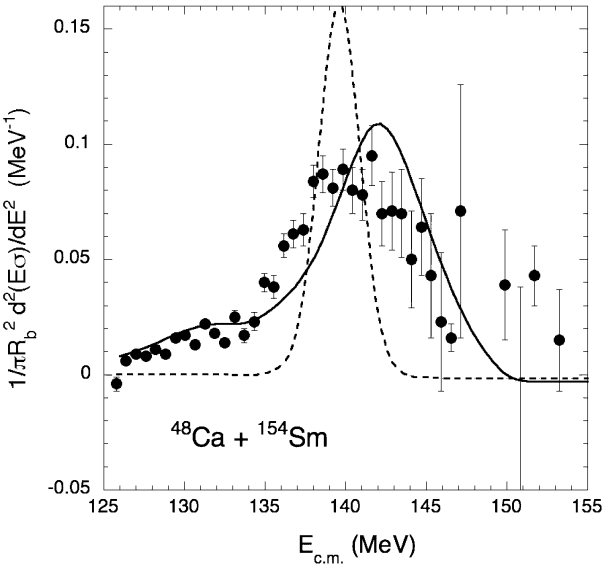

Fig. 4. Capture barrier distributions. The full line is the result of the CC calculations discussed in the text. The no-coupling limit (dotted line) has been divided by two for the sake of clarity.

identical there. By increasing the energy, the ER cross-sections reach a wide maximum ($\sigma_{\rm ER} \approx 100\,$mb) around $E_{\rm cm} \simeq 152$–$154\,$MeV, and then decrease slowly, being only one tenth of the capture cross-section well above the barrier. By differentiating twice the quantity $E\sigma$ (energy × capture cross-section) with respect to the energy, one obtains the usual representation of the *capture* barrier distribution. The result is reported in fig. 4. Here a point-difference formula was used [1], with an energy step of 2.4 MeV.

The barrier distribution is very wide ($\simeq$ 20–22 MeV) and extends down to about 125 MeV, *i.e.* $\simeq 15\,$MeV below the nominal Coulomb barrier. The asymmetry of the barrier distribution shape towards low energies is typical of the collision of a rigid spherical nucleus with a prolate deformed target as ^{154}Sm. We notice that in the Canberra experiment of some years ago on ^{16}O + ^{154}Sm fusion [13], a barrier distribution width $\simeq$ 8–9 MeV was observed. In the present case, channel couplings are stronger and produce a barrier distribution approximately wider by the factor 20/8, since coupling strengths are proportional to $\beta Z_{\rm proj} Z_{\rm targ}$.

3.1 Coupled-channels calculations

The analysis of capture cross-sections and barrier distribution has been performed using the coupled-channel model with the code CCFULL [27]. In CCFULL the number of CC equations is reduced by means of the isocentrifugal approximation, and an incoming-wave boundary condition is placed inside the barrier. It has become clear that simple linear couplings and the adiabatic approximation fail to describe the dynamics of heavy-ion subbarrier fusion [28–30]. Hence CCFULL includes the effects of inelastic non-linear couplings to all orders, and takes full account of the finite excitation energies of the coupled modes. Vibrational couplings are treated in the harmonic limit. The potential we used in the present CC calculations was chosen by fitting the capture cross-sections in the range of 200–400 mb. We remind that the Akyüz-Winther potential parameters [31] for ^{48}Ca + ^{154}Sm are $V_0 = 78.8\,$MeV, $r_0 = 1.18\,$fm and $a = 0.69\,$fm. The corresponding potential barrier has $V_b = 139.6\,$MeV, $R_b = 11.95\,$fm and $\hbar\omega = 3.64\,$MeV (very similar to the Bass barrier [26]).

Our potential requires a barrier near to the Akyüz-Winther estimate and a diffuseness $a \simeq 0.85$. Larger values of the diffuseness, as suggested by the systematic investigation of ref. [32], do not make the situation better, even by readjustments of V_0 and/or r_0 within reasonable ranges. The radius parameter has to be in the vicinity of $r_0 = 1.05\,$fm. As a consequence, a deep potential well ($V_0 = 200\,$MeV) is needed, which, in any case, ensures the applicability of the ingoing-wave boundary condition. The barrier parameters for this potential are $V_b = 139.6\,$MeV, $R_b = 11.82\,$fm and $\hbar\omega = 3.56\,$MeV.

The present potential contains the effect of all channels not included in the CC coupling scheme, as, *e.g.*, the (weak) high-lying quadrupole and octupole vibrations in ^{48}Ca and possible analogous excitations in ^{154}Sm. Only the low-lying octupole vibration of ^{154}Sm ($E_{\rm exc} = 1.013\,$MeV, $\beta_3 = 0.08$) and its ground-state rotational band ($\beta_2 = 0.31$, $\beta_4 = 0.05$ [12]), up to the 24^+ state, were explicitly included in the present calculations. It was checked that this ensures convergence of the results, in particular that no significant variation of the cross-sections is observed when coupling higher states of the rotational band. Transfer couplings are not expected to be important, since all Q-values for neutron stripping and pickup channels are largely negative. They have not been considered here.

The results of CCFULL for the cross-sections are shown in fig. 3; the no-coupling limit is also shown for reference. There is a reasonably good agreement between data and calculations, even if we notice an underestimation of the data at high energies (by up to $\simeq 15\%$, within the systematic error), and a tendency for the calculated excitation function to fall down too much rapidly below $E_{\rm c.m.} = 128\,$MeV. A comparison with the no-coupling limit allows us to appreciate the very large subbarrier cross-section enhancement for ^{48}Ca + ^{154}Sm.

The calculated barrier distribution has been derived from the excitation function using the same procedure we applied for the experimental data. Figure 4 shows the result. The agreement with data is fairly good, in particular the long tail extending towards low energies and the overall width of the distribution are reproduced. We notice that the main peak is slightly shifted with respect to the data. Should we not consider the octupole vibration of ^{154}Sm in the coupling scheme, the situation becomes worse, *i.e.* the main peak is more shifted to the right, and its width reduces.

Concerning ^{16}O + ^{186}W, the existing fusion excitation function [12,22] (fusion-ER + fusion-fission) was successfully analyzed in [12], and, more recently, in the systematic work of Newton *et al.* [32]. The effect of prolate deformation of ^{186}W, with a negative hexadecapole component, was clearly reflected in the subbarrier cross-sections and in the shape of the barrier distribution. At the three energies ($E_{\rm lab} = 109.7, 115.6, 121.1$) where we have measured the ER cross-sections discussed below, no fission data are available. Consequently, no new fusion cross-section can be added to the excitation function for further analysis.

3.2 Comparison with ^{16}O + ^{186}W

We have considered the capture cross-sections of ^{48}Ca + ^{154}Sm and the fusion cross-sections of ^{16}O + ^{186}W, in the whole energy range, using a representation where the two excitation functions can be directly compared to each other. For this we remind here the well-known Wong formula [33] which is valid both above and below a single potential barrier. It is obtained by assuming a parabolic shape of the barrier top, and by replacing the sum over the transmission coefficients $T_\ell(E)$ by an integral. It reads

$$\sigma = \frac{\hbar\omega R_b^2}{2E \ln(1 + \exp[(2\pi/\hbar\omega)(E - V_b)])}. \quad (1)$$

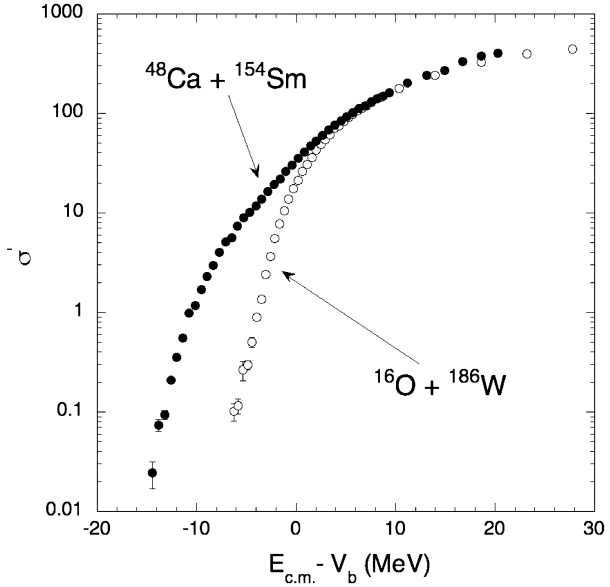

Fig. 5. Modified capture (fusion) cross-sections for ^{48}Ca + ^{154}Sm (^{16}O + ^{186}W) *vs.* the energy distance from the Coulomb barrier. The ordinate σ' is defined by eq. (2) in the text.

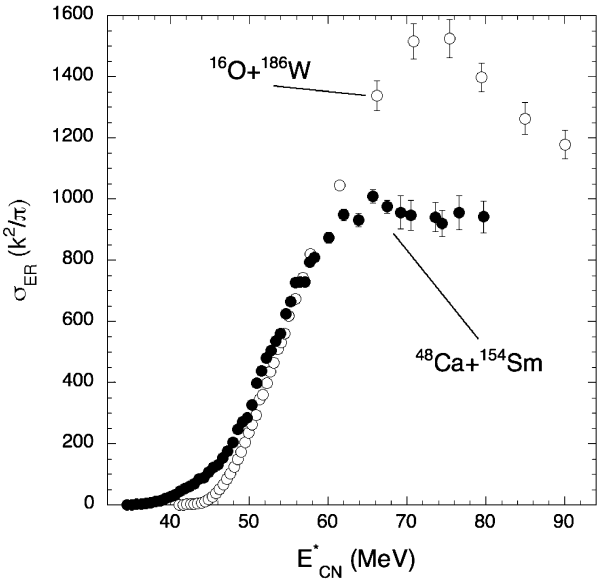

Fig. 6. Excitation functions corresponding to the reduced ER cross-sections for ^{48}Ca + ^{154}Sm (present work) and for ^{16}O + ^{186}W ([12] and present work). The reported errors are purely statistical.

This formula gives the barrier-passing (or capture) cross-section which, in the case of ^{16}O + ^{186}W, coincides with the fusion cross-section, since no indication of quasi-fission exists in that case.

We define

$$\sigma' = \frac{2E\sigma}{\hbar\omega R_b^2} \tag{2}$$

and we use for V_b, R_b and $\hbar\omega$ the values obtained from the potentials of the CC calculations described above and in ref. [32], which best fit the data for $\sigma \simeq 200$ mb. We notice that the barrier curvatures $\hbar\omega$ are very similar for the two systems considered here ($\hbar\omega$ is 3.56 MeV and 3.50 MeV for ^{48}Ca + ^{154}Sm and for ^{16}O + ^{186}W, respectively). Therefore, the modified cross-section σ' should be *almost* the same in both cases, at the same distance from the barrier, if no coupling effects modify the situation. Relative subbarrier enhancements of one system with respect to the other can be readily put in evidence in a plot of σ' *vs.* $E - V_b$. This is shown in fig. 5. In the region above the barrier the cross-sections are very similar for the two systems, as it is obvious to expect. Subbarrier cross-sections show the much stronger coupling effects in the heavier and more mass-symmetric system, although the prolate deformations of ^{154}Sm and ^{186}W are quite comparable. We can clearly deduce from fig. 5 that more of the barrier strength is moved to lower energies in the ^{48}Ca + ^{154}Sm case.

Far below the barrier, the relative enhancement is in excess of two orders of magnitude. This is much more than any reasonably expected fusion hindrance phenomenon in the more mass-symmetric system ^{48}Ca + ^{154}Sm, in that energy region.

4 Evaporation residue cross-sections

We analyze now the measured ER cross-sections for the two systems near and above the Coulomb barrier. This will allow us to obtain interesting information on the dynamics of the reactions after that capture inside the barrier has taken place.

In order to compare ER cross-sections $\sigma_{\rm ER}$ for different systems leading to the same CN, where the capture cross-sections can be different due a variery of reasons (different Coulomb barriers, coupling effects, etc.), it is appropriate to use a representation of *reduced* cross-sections [5,10,11,21,34] *vs.* CN excitation energy $E^*_{\rm CN} = E^*$. Figure 6 is this kind of plot for the two systems we are considering. The reduced ER cross-section $\tilde{\sigma}_{\rm ER} = \sigma_{\rm ER} \times (k^2/\pi)$, where k is the wave number, can be written as

$$\tilde{\sigma}_{\rm ER} = \sum_{\ell} (2l+1) T_\ell(E) P_{\rm CN}(\ell, E^*) P_{\rm sur}(\ell, E^*), \tag{3}$$

where $T_\ell(E)$ is the transmission coefficient for the partial wave ℓ at the energy E, $P_{\rm CN}(\ell, E^*)$ is the probability that the CN is formed starting from a di-nucleus configuration (from capture inside the barrier), and $P_{\rm sur}(\ell, E^*)$ is the probability that the CN survives against fission. Both probabilities are ℓ- and E^*-dependent.

Following the underlying assumption of the validity of Bohr's hypothesis that CN decay is independent of the way it was formed, $P_{\rm sur}(\ell, E^*)$ does not depend on the entrance channel. Hence, if no hindrance to fusion were present (*i.e.* $P_{\rm CN}(\ell, E^*) = 1$), plotting $\tilde{\sigma}_{\rm ER}$ *vs.* $E^*_{\rm CN}$ should show identical reduced cross-sections for the two systems, above a critical energy where $T_\ell \simeq 1$ for all partial waves

leading to ER production. In other words, when such partial waves are fully populated, the yield of ER saturates and $T_\ell = 1$ can be dropped from the formula. This is the case above $E^*_{\rm CN} \simeq 70$–$72\,{\rm MeV}$ (see fig. 6).

Figure 6 shows actually that, around $E^*_{\rm CN} = 72\,{\rm MeV}$ and above, the $^{48}{\rm Ca} + {}^{154}{\rm Sm}$ reduced cross-sections are smaller by $\approx 40\%$ with respect to $^{16}{\rm O} + {}^{186}{\rm W}$. The evidence is that, in analogy with the cases of production of heavier compound nuclei ($^{216}{\rm Ra}^*$ and $^{220}{\rm Th}^*$) studied recently [10,11], the fusion of $^{48}{\rm Ca} + {}^{154}{\rm Sm}$ leading to $^{202}{\rm Pb}^*$ is inhibited, due to the presence of quasi-fission [23], for the low partial waves associated to the production of ER. A comprehensive statistical-model analysis of the present data, together with those on CN fission and quasi-fission, is in progress. This analysis will be presented elsewhere, and it will hopefully lead to a better understanding of the reaction dynamics for the relatively heavy $^{48}{\rm Ca} + {}^{154}{\rm Sm}$ system from well below to well above the barrier.

Indeed, the comparison of fig. 6 is model independent, but it cannot tell us much about the situation below the critical energy $E^*_{\rm CN} \simeq 70$–$72\,{\rm MeV}$, even if, qualitatively speaking, it is likely that an inhibition exists at lower energies too. In any case, we have learnt from the analyses of the previous sections that channel-coupling effects are very strong for $^{48}{\rm Ca} + {}^{154}{\rm Sm}$. Therefore, any realistic fusion hindrance below the barrier would be more than counterbalanced by the competing orders-of-magnitude subbarrier enhancements.

Of course, processes such as pre-equilibrium charged-particle emission and incomplete fusion will be different in the two entrance channels [11,35], the former being more important for $^{48}{\rm Ca} + {}^{154}{\rm Sm}$ and the latter more important for $^{16}{\rm O} + {}^{186}{\rm W}$. This should be taken into account in high-resolution studies of mass and Z distributions of evaporation residues. Such processes cannot be discriminated in our experiments and could not be corrected for in the data analysis by, *e.g.*, selecting xn evaporation channels only (cf. sect. 2.1). It has to be pointed out, however, that incomplete fusion does not appear to be significant for $^{16}{\rm O} + {}^{186}{\rm W}$ in the energy range we are discussing (see [36] and references therein), where the fusion excitation function is nicely reproduced by the CC calculations with potential parameters following the recent systematics [32] quite well.

5 Summary and conclusions

We have measured fusion-evaporation cross-sections for the system $^{48}{\rm Ca} + {}^{154}{\rm Sm}$ in an energy range from $\simeq 11\%$ below to $\simeq 20\%$ above the Coulomb barrier. The excitation function for capture (barrier-passing) has been derived by adding recently measured capture-fission cross-sections, in the same energy range, to the present ER cross-sections. The barrier distribution has been extracted as the second energy derivative of the capture excitation function. The distribution extends down to $\simeq 15\,{\rm MeV}$ below the Coulomb barrier, and is typical of the collision of a spherical rigid nucleus like $^{48}{\rm Ca}$ with a prolate deformed target as $^{154}{\rm Sm}$.

Both capture cross-sections and barrier distribution have been compared to the predictions of coupled-channel calculations where the static deformation of $^{154}{\rm Sm}$ has been taken into account. A good description of the experimental data has been obtained, and a large subbarrier cross-section enhancement is clearly seen. Actually, a simple comparison with the fusion excitation function of $^{16}{\rm O} + {}^{186}{\rm W}$ leading to the same compound nucleus $^{202}{\rm Pb}^*$, shows a large relative subbarrier enhancement in favour of $^{48}{\rm Ca} + {}^{154}{\rm Sm}$.

For $^{16}{\rm O} + {}^{186}{\rm W}$ we have measured ER cross-sections at a few energies higher than what available in the literature [12,22]. Comparing the $^{48}{\rm Ca} + {}^{154}{\rm Sm}$ ER cross-sections to the corresponding ones for $^{16}{\rm O} + {}^{186}{\rm W}$ in a reduced scale, reveals that fusion is relatively inhibited for $^{48}{\rm Ca} + {}^{154}{\rm Sm}$ by at least $\approx 40\%$, for the above-barrier energies around $E^*_{\rm CN} \simeq 72\,{\rm MeV}$. The need for a detailed analysis of ER, CN-fission and quasi-fission cross-sections within the statistical model is clearly felt, so to get a deeper insight into the reaction dynamics after that capture inside the Coulomb barrier has taken place. Such analysis is underway.

$^{48}{\rm Ca} + {}^{154}{\rm Sm}$ is a heavy system where both strong channel couplings and the competing quasi-fission reaction channel are active. Hence we have been able to observe both a very large enhancement and a large inhibition of fusion, in nearby energy ranges. For very heavy systems where channel couplings may be even stronger, but where quasi-fission becomes at the same time largely dominating, a very careful choice of the bombarding energy and of the projectile-target combination is necessary for the production of a compound nucleus, taking into account also the capture barrier distribution.

Grateful thanks are due to P. Gomes and A. Szanto de Toledo for participating in one of the experiments. We are pleased to acknowledge the professional work of Mr. G. Binelle, Mr. G. Manente and Mr. M. Loriggiola in the preparation of beams and targets of excellent quality, and of the XTU Tandem-ALPI staff for careful and patient work during the experiments.

References

1. M. Dasgupta, D.J. Hinde, N. Rowley, A.M. Stefanini, Annu. Rev. Nucl. Part. Sci. **48**, 401 (1998).
2. A.B. Balantekin, N. Takigawa, Rev. Mod. Phys. **70**, 77 (1998).
3. K.H. Schmidt, W. Morawek, Rep. Prog. Phys. **54**, 949 (1991).
4. W. Reisdorf, J. Phys. G: Nucl. Part. Phys. **20**, 1297 (1994).
5. C.-C. Sahm, H.G. Clerc, K.-H. Schmidt, W. Reisdorf, P. Armbruster, F.P. Hessberger, J.G. Keller, G. Münzenberg, D. Vermeulen, Nucl. Phys. A **441**, 316 (1985).
6. W.J. Swiatecki, Nucl. Phys. A **376**, 275 (1982); Phys. Scr. **24**, 113 (1981).
7. S. Bjornholm, W. Swiatecki, Nucl. Phys. A **391**, 471 (1982).

8. J.P. Blocki, H. Feldmeier, W.J. Swiatecki, Nucl. Phys. A **459**, 145 (1986).
9. B.B. Back, P.B. Fernandez, B.G. Glagola, D. Henderson, S. Kaufman, J.G. Keller, S.J. Sanders, F. Videbaek, T.F. Wang, B.D. Wilkins, Phys. Rev. C **53**, 1734 (1996).
10. A.C. Berriman, D.J. Hinde, M. Dasgupta, C.R. Morton, R.D. Butt, J.O. Newton, Nature (London) **413**, 144 (2001).
11. D.J. Hinde, M. Dasgupta, A. Mukherjee, Phys. Rev. Lett. **89**, 282701 (2002).
12. J.R. Leigh, M. Dasgupta, D.J. Hinde, J.C. Mein, C.R. Morton, R.C. Lemmon, J.P. Lestone, J.O. Newton, H. Timmers, J.X. Wei, N. Rowley, Phys. Rev. C **52**, 3151 (1995).
13. J.X. Wei, J.R. Leigh, D.J. Hinde, J.O. Newton, R.C. Lemmon, S. Elfström, J.X. Chen, N. Rowley, Phys. Rev. Lett. **67**, 3368 (1991).
14. S. Mitsuoka, H. Ikezoe, K. Nishio, J. Lu, Phys. Rev. C **65**, 054608 (2002).
15. D.J. Hinde, M. Dasgupta, J.R. Leigh, J.C. Mein, C.R. Morton, J.O. Newton, H. Timmers, Phys. Rev. C **53**, 1290 (1996).
16. H. Timmers, D. Ackermann, S. Beghini, L. Corradi, J.H. He, G. Montagnoli, F. Scarlassara, A.M. Stefanini, N. Rowley, Nucl. Phys. A **633**, 421 (1998).
17. C.R. Morton, A.C. Berriman, M. Dasgupta, D.J. Hinde, J.O. Newton, K. Hagino, I.J. Thompson, Phys. Rev. C **60**, 044608 (1999).
18. M. Trotta, A.M. Stefanini, L. Corradi, A. Gadea, F. Scarlassara, S. Beghini, G. Montagnoli, Phys. Rev. C **65**, 011601(R) (2001).
19. K. Satou, H. Ikezoe, S. Mitsuoka, K. Nishio, S.C. Jeong, Phys. Rev. C **65**, 054602 (2002).
20. H. Ikezoe, K. Satou, S. Mitsuoka, K. Nishio, K. Tsuruta, S.C. Jeong, C.J. Lin, *Proceedings of the International Conference FUSION03, Matsushima, Japan, November 12-15, 2003*, Prog. Theor. Phys. Suppl. **154**, 45 (2004).
21. R.N. Sagaidak, G.N. Kniajeva, I.M. Itkis, M.G. Itkis, N.A. Kondratiev, E.M. Kozulin, I.V. Pokrovsky, A.I. Svirikhin, V.M. Voskressensky, A.D. Yeremin, L. Corradi, A. Gadea, A. Latina, A.M. Stefanini, S. Szilner, M. Trotta, A.M. Vinodkumar, S. Beghini, G. Montagnoli, F. Scarlassara, D. Ackermann, F. Hanappe, N. Rowley, L. Stuttge, Phys. Rev. C **68**, 014603 (2003).
22. C.E. Beamis, T.C. Awes, J.R. Beene, R.L. Ferguson, H.J. Kim, F.K. McGowan, F.E. Obershain, F. Plasil, P. Jacobs, Z. Frankel, U. Smilanski, I. Tserruya, ORNL Physics Division Progress Report No. **6326**, 110 (1986).
23. M. Trotta *et al.*, Nucl. Phys. A **734**, 245 (2004); Prog. Theor. Phys. Suppl. **154**, 37 (2004).
24. A.M. Stefanini, D. Ackermann, L. Corradi, D.R. Napoli, C. Petrache, P. Spolaore, P. Bednarczyk, H.Q. Zhang, S. Beghini, G. Montagnoli, L. Mueller, F. Scarlassara, G.F. Segato, F. Soramel, N. Rowley, Phys. Rev. Lett. **74**, 864 (1995).
25. S. Beghini, C. Signorini, S. Lunardi, M. Morando, G. Fortuna, A.M. Stefanini, W. Meczynski, R. Pengo, Nucl. Instrum. Methods A **239**, 585 (1985).
26. R. Bass, Lect. Notes Phys. **117**, 281 (1980).
27. K. Hagino, N. Rowley, A.T. Kruppa, Comput. Phys. Commun. **123**, 143 (1999).
28. H. Esbensen, S. Landowne, Phys. Rev. C **35**, 2090 (1987).
29. H. Esbensen, B.B. Back, Phys. Rev. C **54**, 3109 (1996).
30. K. Hagino, N. Takigawa, M. Dasgupta, D.J. Hinde, J.R. Leigh, Phys. Rev. C **55**, 276 (1997).
31. Ö. Akyüz, A. Winther, in *Nuclear Structure and Heavy-Ion Physics, Proceedings of the International School of Physics Enrico Fermi, Varenna, Course LXXVII*, edited by R.A. Broglia, R.A. Ricci (North-Holland, Amsterdam, 1981).
32. J.O. Newton, R.D. Butt, M. Dasgupta, D.J. Hinde, I.I. Gontchar, C.R. Morton, K. Hagino, Phys. Rev. C **70**, 024605 (2004).
33. C.Y. Wong, Phys. Rev. Lett. **31**, 766 (1973).
34. W. Reidorf, F.P. Hessberger, K.D. Hildenbrand, S. Hofmann, G. Münzenberg, K.-H. Schmidt, W.F.W. Schneider, K. Sümmerer, G. Wirth, J.V. Kratz, K. Schlitt, C.-C. Sahm, Nucl. Phys. A **444**, 154 (1985).
35. H. Feldmeier, Rep. Prog. Phys. **50**, 915 (1987).
36. P. Vergani, E. Gadioli, E. Vaciago, E. Fabrici, E. Gadioli Erba, M. Galmarini, G. Ciavola, C. Marchetta, Phys. Rev. C **48**, 1815 (1993).